Characterization of Rat Optic Nerve Head (ONH) Biomechanics through Finite Element (FE) and Sensitivity Analysis of Tissues

A Thesis
Presented to
The Academic Faculty

by

Alison Kight

In Partial Fulfillment
of the Requirements for the Degree
Bachelor of Science in Biomedical Engineering in the
Wallace H. Coulter Department of Biomedical Engineering at the Georgia Institute of Technology

Georgia Institute of Technology
December 4, 2017

Characterization of Rat Optic Nerve Head (ONH) Biomechanics through Finite Element (FE) and Sensitivity Analysis of Tissues

Approved by:

Professor C. Ross Ethier, Advisor
Wallace H. Coulter Department of Biomedical Engineering
Georgia Institute of Technology and Emory University

Dr. Andrew Feola,
Wallace H. Coulter Department of Biomedical Engineering
Georgia Institute of Technology and Emory University

Date Approved: December 4, 2017

Characterization of Rat Optic Nerve Head (ONH) Biomechanics through Finite Element (FE) and Sensitivity Analysis of Tissues

Approved by:

Professor C. Ross Ethier, Advisor
Wallace H. Coulter Department of
Biomedical Engineering
Georgia Institute of Technology and Emory University

Dr. Andrew Feola,
Wallace H. Coulter Department of
Biomedical Engineering
Georgia Institute of Technology and Emory University

Date Approved: December 4, 2017

Table of Contents

ACKNOWLEDGEMENTS

I wish to thank Stephen Schwaner, PhD candidate at the Georgia Institute of Technology, for being patient, informative, and extremely helpful throughout this research.

LIST OF SYMBOLS AND ABBREVIATIONS

A	Anterior
BM	Bruch's Membrane
BMO	Bruch's Membrane Opening
BP	Blood Pressure
CRA	Central Retinal Artery
CRV	Central Retinal Vein
FE	Finite Element
FEM	Finite Element Modeling
IAC	Inferior Arterial Canal
N	Nasal
IOP	Intraocular Pressure
ONH	Optic Nerve Head
PNVP	Perineural Vascular Plexus
P	Posterior
RGC	Retinal Ganglion Cell
T	Temporal

SUMMARY

Glaucoma, the second leading cause of blindness, is characterized by the death of retinal ganglion cells (RGCs). The pathophysiology of glaucoma is complicated, and the cellular mechanisms behind it are poorly understood. Studies have shown that the optic nerve head (ONH) is the primary site of damage in glaucoma, and that critical deformation in the ONH from increased intraocular pressure (IOP) can contribute to RGC loss. Thus, biomechanics provides an important and quantitative framework that can describe and analyze how IOP-induced strain in ONH tissues induces and influences the pathophysiology of glaucoma. Experimental animal models of glaucoma, specifically rat models, are also useful tools for gaining insight into how elevated IOP can lead to the pathophysiology of glaucoma. To determine how biomechanics affects glaucoma pathophysiology, biomechanical characterizations are needed for each glaucoma animal model. Although the experimental rat model for glaucoma is widely used, its ONH biomechanics have not been characterized. This research aims to characterize the rat ONH biomechanical environment by building individual-specific rat ONH finite element models. We will also conduct a sensitivity analysis to determine which tissue material properties have the largest effect on IOP-induced mechanical strain in the ONH. Analysis of the data will include a qualitative look at strain fields and patterns as well as a quantitative look at first and third principal strains in the anterior region of the ONH. A sensitivity analysis on the rat ONH model will vary the material properties of tissues and determine their influence on the overall strain in the optic nerve head under increased IOP. Results from each individual specific model will improve understanding of how biomechanical insult due to elevated IOP to the rat ONH may affect glaucoma pathophysiology and identify which tissues biomechanical properties may lead to large ONH deformation due to elevated IOP.

1 INTRODUCTION

Glaucoma is the second leading cause of blindness, affecting over 70 million individuals worldwide. Glaucoma is characterized by the death of retinal ganglion cells (RGCs), which carry visual information from the retina to the brain. Studies have shown that the optic nerve head (ONH) is the primary site of damage in glaucoma. Specifically, biomechanical tension and compression resulting from increased intraocular pressure (IOP) are theorized to critically deform ONH tissues, leading to RGC death. Biomechanics provides a key and quantitative framework that can describe and analyze how IOP-induced strains in ONH tissues induce and influence the pathophysiology of glaucoma.

Glaucoma is complicated, and the cellular mechanisms leading from biomechanical insult to RGC death are poorly understood. Animal models are commonly used to learn more about the complex glaucoma pathophysiology. One such model, the nonhuman primate, has several advantages for studying glaucoma, including the fact that its ONH anatomy closely matches that of the human. However, due to the high cost, highly specialized care, and ethical concerns associated with experimenting on nonhuman primates, these models are unrealistic for detailed studies on the cellular processes occurring in glaucoma, as these types of studies require high subject numbers. Studying rodent glaucoma models is a promising alternative. Currently, there is a substantial amount of experimental data on the cellular processes in the rat model of glaucoma. Additionally, there are similar damage patterns in the rat model of glaucoma compared to human glaucoma.

However, the rat and human ONH anatomy are significantly different. Understanding these differences is critical to our use of the rat model of glaucoma, as they are likely to affect the

biomechanics of the rat ONH. Therefore, this research aims to characterize rat ONH biomechanics by developing individual-specific finite element (FE) models of rat ONHs and using them to perform sensitivity analyses. FE analysis is a computational technique that allows users to solve biomechanical problems involving complex geometries and loading conditions. Furthermore, sensitivity analyses on the rat ONH FE models can determine the level of influence of tissue material properties on the strains in the ONH under increased IOP. Understanding strain patterns in the rat ONH will allow for a better interpretation of data from rat studies of glaucoma and increase understanding of the role of biomechanics in glaucomatous RGC death.

2 BACKGROUND

2.1 Glaucoma

Glaucoma is the second leading cause of blindness, and current therapies are not always effective [1]. Though the complex cellular mechanisms behind the pathophysiology are poorly understood, research has suggested that increased intraocular pressure is critical to the onset of the disease [2], which implicates biomechanics in the pathophysiology of the disease. Studies have shown that the optic nerve head (ONH) is the primary site of damage in glaucoma [3]. Specifically, biomechanical tension and compression resulting from increased intraocular pressure (IOP) are theorized to critically deform ONH tissues, leading to RGC death. As shown in Figure 2.1, RGC nerve fibers run through the lamina cribrosa, a mesh-like connective tissue structure that spans the scleral canal. This anatomy is critical to the onset of the disease.

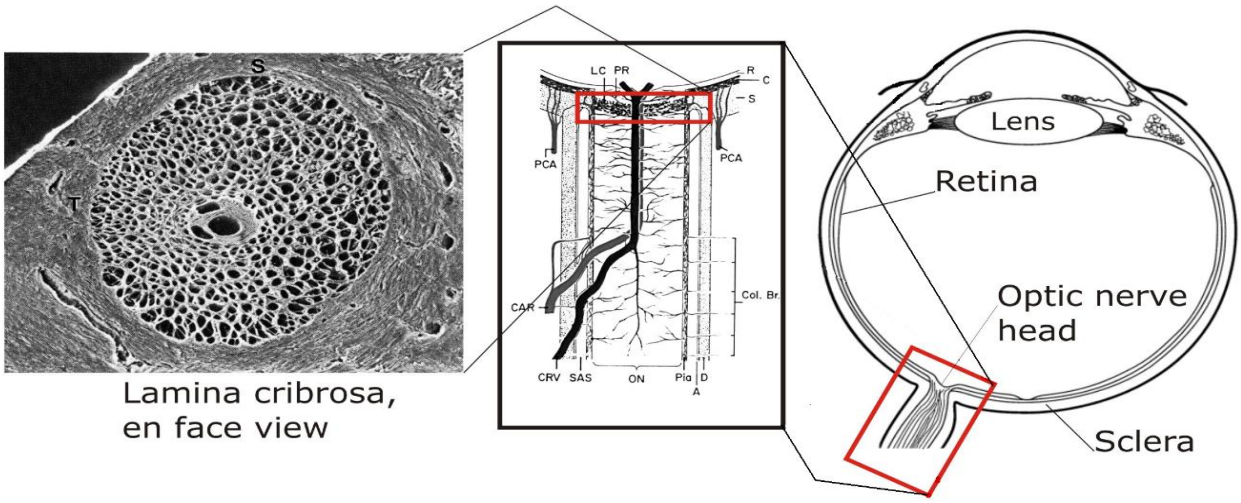

Figure 2.1. (Left to Right) Electron microscopic image of the lamina cribrosa, schematic of the ONH, and schematic of the eye anatomy [5]. All three represent human anatomy.

2.2 The Experimental Rat Model of Glaucoma

Understanding the pathophysiology of glaucoma requires highly controlled studies with high sample numbers. Thus, studying donated human eyes is useful but not sufficient for this purpose. This makes animal models useful for investigating the cellular mechanisms in glaucoma.

The nonhuman primate model of glaucoma closely replicates human glaucoma pathophysiology, and ONH anatomy of both species is nearly identical. However, this model is unrealistic for use on a large scale. In order to overcome this obstacle, rat glaucoma models show promising advantages. There is already a substantial amount of data on biomolecular and cellular processes of rats in glaucoma. Additionally, rat studies have shown that similar damage patterns occur as in human glaucoma, such as RGC apoptosis and the ONH as the initial site of damage [6][7].

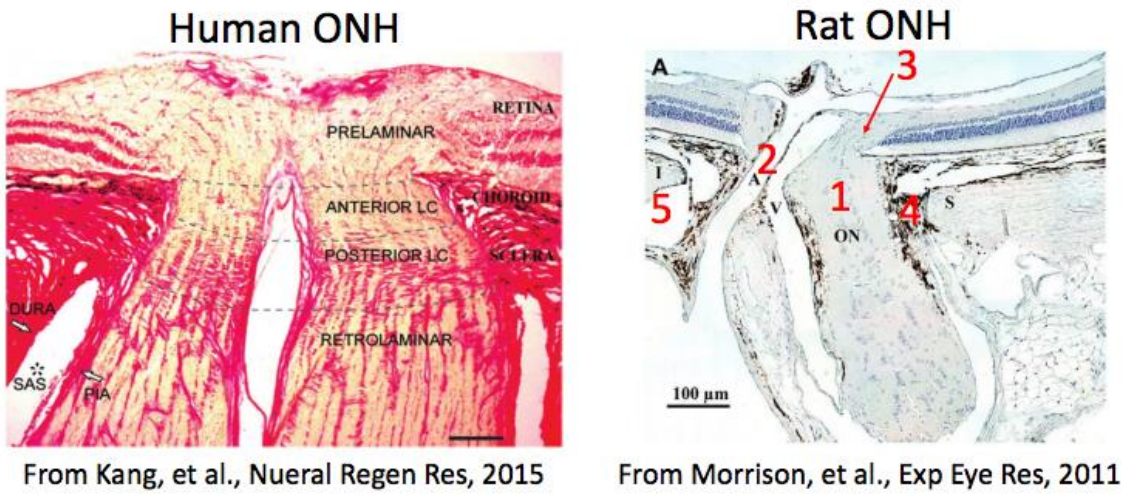

Figure 2.2. Comparison between rat [8] and human ONH [13].

However, there are significant anatomic differences between the rat and human ONH [8]. The main differences include (shown in figure 2.2):

1. Lack of collagenous lamina cribrosa in the rat eye.

2. The inferior placement rather than central placement of the main artery and vein that pass through the nerve as it leaves the globe.

3. Bruch's membrane (a connective tissue membrane that separates the choroid and retina) in the rat eye juts more extremely into the nerve tissue on the superior side of the nerve.

4. The existence of a perineural vascular plexus in between the nerve and the sclera, particularly on the superior side of the nerve.

5. The existence of an inferior arterial canal in the rat sclera, located inferior to the nerve.

Since there are a number of differences between the human and rat ONH anatomy it is important to understand how these may affect the biomechanics of the tissue. Therefore it is necessary to develop specific and accurate characterizations of the strain profiles in rat ONH.

2.3 Finite Element Modeling of ONH Biomechanics

There is good evidence that biomechanical damage to the ONH is a primary factor in glaucoma pathophysiology [9]. Elevated IOP is a key factor in the onset of the damage, but the mechanisms by which elevated IOP leads to RGC death is not well-understood. In addition, IOP susceptibility varies between individuals, making biomechanical analysis of the ONH tissues critical to the overall understanding of glaucoma. Strain, or elongation, of tissues is important in biomechanical analysis because studies have shown that cells are mechanosensitive and respond to deformation. Higher levels of strain can cause direct mechanical insult, so characterizations of strain patterns in the ONH is critical.

FE modeling is a key tool in understanding the complex biomechanics of the ONH. Sigal et al. demonstrates the merit of FE modeling and various tissue sensitivity analyses methods through several computer models of human ONHs [11] [12]. Most notably, it was found that scleral stiffness was the most influential mechanical factor. Thus, characterization of the biomechanics of the sclera and surrounding tissue environment are imperative to understanding ocular neuropathy. However, this type of individual-specific FEM and sensitivity analysis of tissues for the rat ONH has yet to be done, and biomechanical characterizations of the rat ONH model are needed to better interpret data from experimental rat studies of glaucoma.

2.4 Purpose

Though useful, non-human primate models of glaucoma are not practical for use in detailed cell biology studies due to their high cost and need for highly specialized animal facilities. Thus, rodent models have been utilized to better understand the cellular pathophysiology of glaucoma, particularly in the ONH. However, the rat ONH is anatomically different from the human ONH, and these differences highlight the need for characterization of rat ONH biomechanics. It is likely these differences influence the biomechanics and thus the pathogenesis of RGCs. Therefore, a biomechanical characterization of the rat ONH is necessary to better understand rat glaucoma studies. Further, comparison of biomechanical data, such as stress and strain, to patterns of cell response from rat glaucoma studies, can provide insight into how biomechanics influences RGC death in glaucoma. This research aims to characterize the biomechanics of the rat ONH through FE modeling and sensitivity analyses of relevant ONH tissues.

3 METHODS AND MATERIALS

3.1 Individual Specific Model Building

Building rat ONH finite element models requires three main steps: acquisition of rat ONH tissue geometry data, model geometry building, and model geometry meshing. The Burgoyne lab in Portland, Oregon has collected 3D rat ONH geometry data using a custom histomorphometry technique and software (Multiview) [17]. Each rat eye was perfusion fixed at an IOP of 10 mmHg. A 3 mm trephine was used to remove the peripapillary sclera on the ONH. Each eye was embedded in paraffin and serial sectioned at a resolution of 1.5 microns using a microtome. After each cut was made, the block face was marked with a connective tissue stain and a picture was taken at 1.5 x 1.5 micrometers per pixel. All digital transverse section images were combined in an image stack, producing a 3D reconstruction of rat ONH tissue morphology. Multiview allows the user to view any desired radial or transverse section through this 3D reconstruction. The program also allows the user to manually delineate the boundaries of the key tissues passing through each viewed section.

3.1.1 Multiview

Tissue delineations of several ocular structures were previously done by the Burgoyne lab (Figure 3.1) and slightly adjusted for the purposes of modeling (Figure 3.2). These small adjustments did not alter tissue geometry but were necessary to allow for model building and subsequent meshing. The sclera, Bruch's Membrane (BM), nerve, and pia mater were delineated by viewing radial sections. The branching sections of the central retinal vein (CRV) were delineated in this manner as well, when necessary. The central branch of the CRV, the central retinal artery (CRA), and the inferior arterial canal (IAC) were delineated using transverse cross sectional views (Figure 3.3).

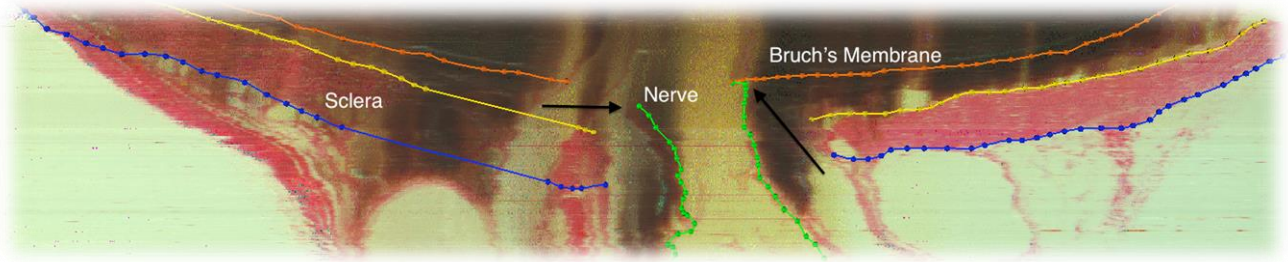

Figure 3.1. Burgoyne Lab delineations of the sclera, nerve, and Bruch's membrane.

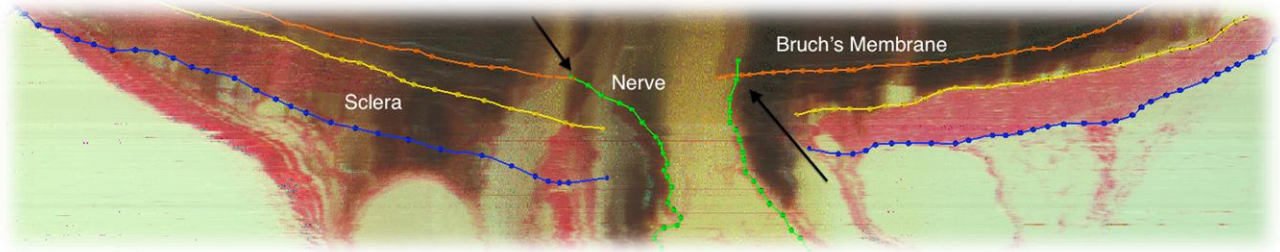

Figure 3.2. Changes made to Burgoyne lab delineation data in default mode. Arrows indicate location of changes.

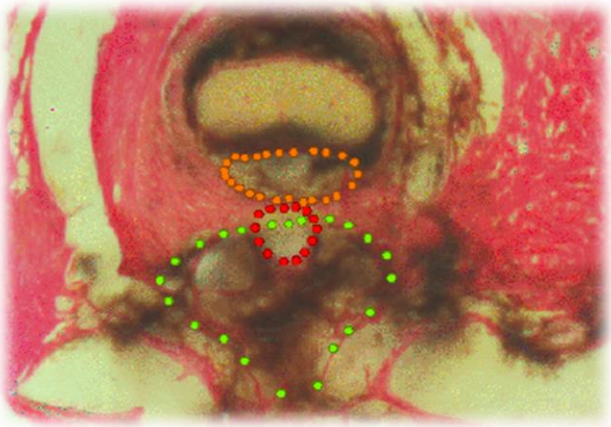

Figure 3.3. Delineation of vessels and inferior canal using a transverse cross section: CRV (orange), CRA (red), IAC (green).

3.1.2 Geometry

Points from Multiview were exported into Rhino (Robert McNeel & Associates, Seattle, WA, Rhino 5.0; see Figure 3.4). Building model geometry required fitting surfaces to point cloud data and then combining those surfaces to produce a volume representing each ONH tissue.

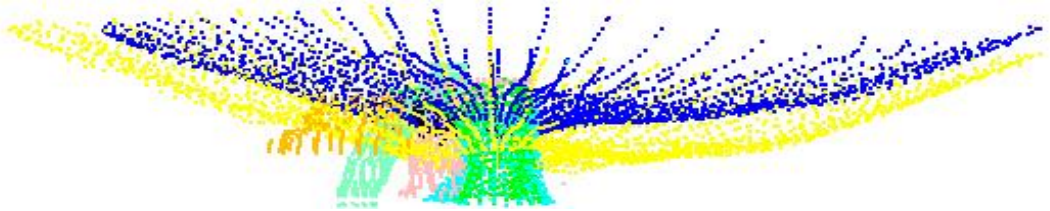

Figure 3.4. Point clouds of the various tissue delineations exported from Multiview into Rhino.

3.1.2.1 Surfaces

The CRA and CRV points were surfaced using a Rhino script (see Figure 3.5 for CRA surface). The thickness of these vessels were accounted for by offsetting the surfaces 10 µm and 3 µm for the CRA and CRV respectively. The IAC points were also surfaced using the same Rhino script. The CRV was surfaced in four sections: anterior, nasal branch, temporal branch, and posterior. Using the Rhino plugin T-splines (Autodesk Inc), the sections were manually merged together to create a single polysurface (see Figure 3.6). The nerve was surfaced using cross-sectional views to create curves around the points and then lofting those curves into a polysurface (see Figure 3.7). The inner layer of the pia mater was made from the nerve surface, and the outer layer was a T-spline offset of 20 micrometers, which was then manually adjusted to fit the points from Multiview. A surface was then fit to the BM points and offset 3 micrometers to provide a suitable thickness (see Figure 3.8). Surfaces were fit to the anterior and posterior scleral points. The choroid was formed from the anterior scleral surface and the posterior BM surface. The perineural vascular plexus (PNVP) was formed from curves fit to the anterior and posterior scleral canal opening points. The "sweep 2 rail" command in Rhino created the surface shared between the sclera and PNVP. The thickness for the vessels, pia, and BM were based on previous data measured from histology slides.

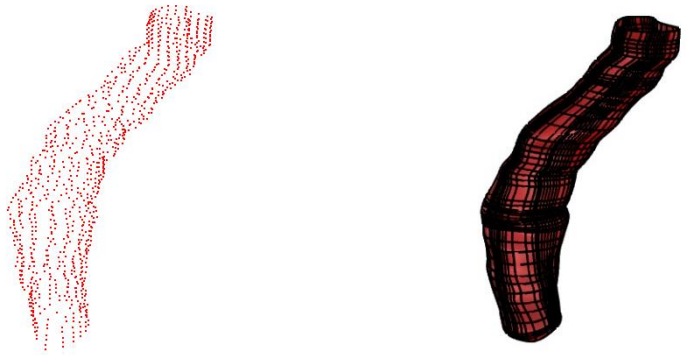

Figure 3.5. Surfacing of the CRA on Rhino from imported points on Multiview.

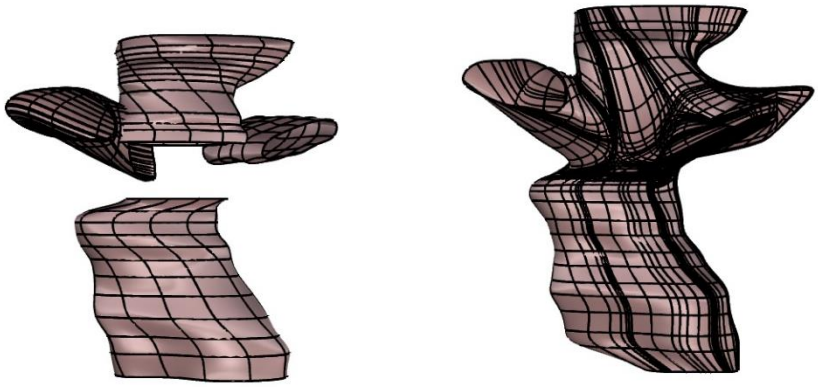

Figure 3.6. Manual connection of branches using t-splines plug-in to create a single CRV polysurface.

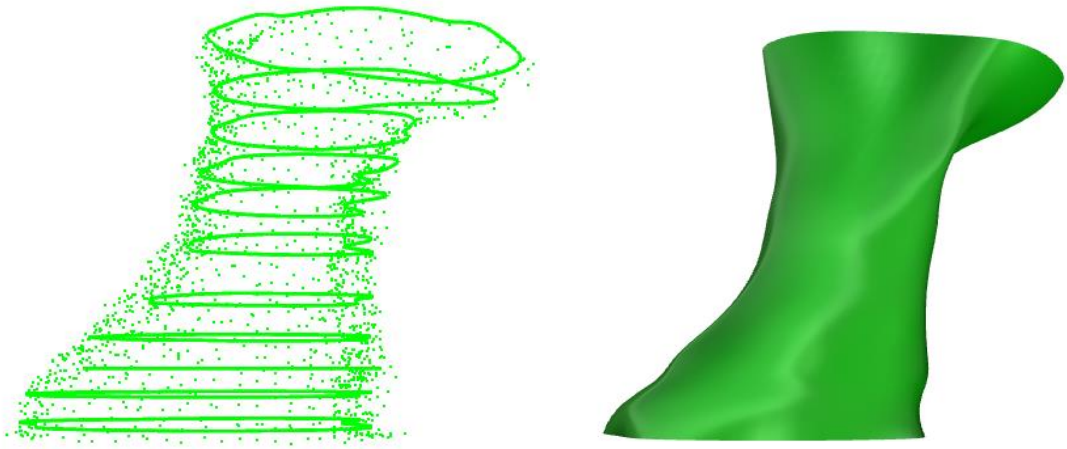

Figure 3.7. Nerve polysurface was created from lofting curves that fit through the imported points.

Figure 3.8. Surfacing of Bruch's Membrane utilizing the "patch" command.

3.1.2.2 Solids

Each tissue was modeled into a watertight solid, or in Rhino terms, a closed polysurface. Finalized solids are shown in Figure 3.7. The CRV and IAC were cut by the CRA (see Figure 3.9). The pia mater was cut by the CRV. The PNVP was cut by the pia mater and CRV. Outer

surfaces were added, connecting the anterior and posterior surfaces of the choroid and sclera. In order to make watertight volumes, the tissue volumes passing through the choroid and sclera (such as the CRV, CRA, nerve, etc.) were cut out so that the resulting sclera and choroid were flush with these vessels (see Figures 3.10 and 3.11). CRA, CRV, and nerve tissue portions in the BM-level were created by offsetting the anterior surfaces of each solid 3 microns (Figure 3.12). After the solids were fully completed, a MATLAB code was run to project the modeled tissues back onto the original histology slide to assess how well the model represented the true anatomy (Figure 3.13). The complete model is shown in Figure 3.14.

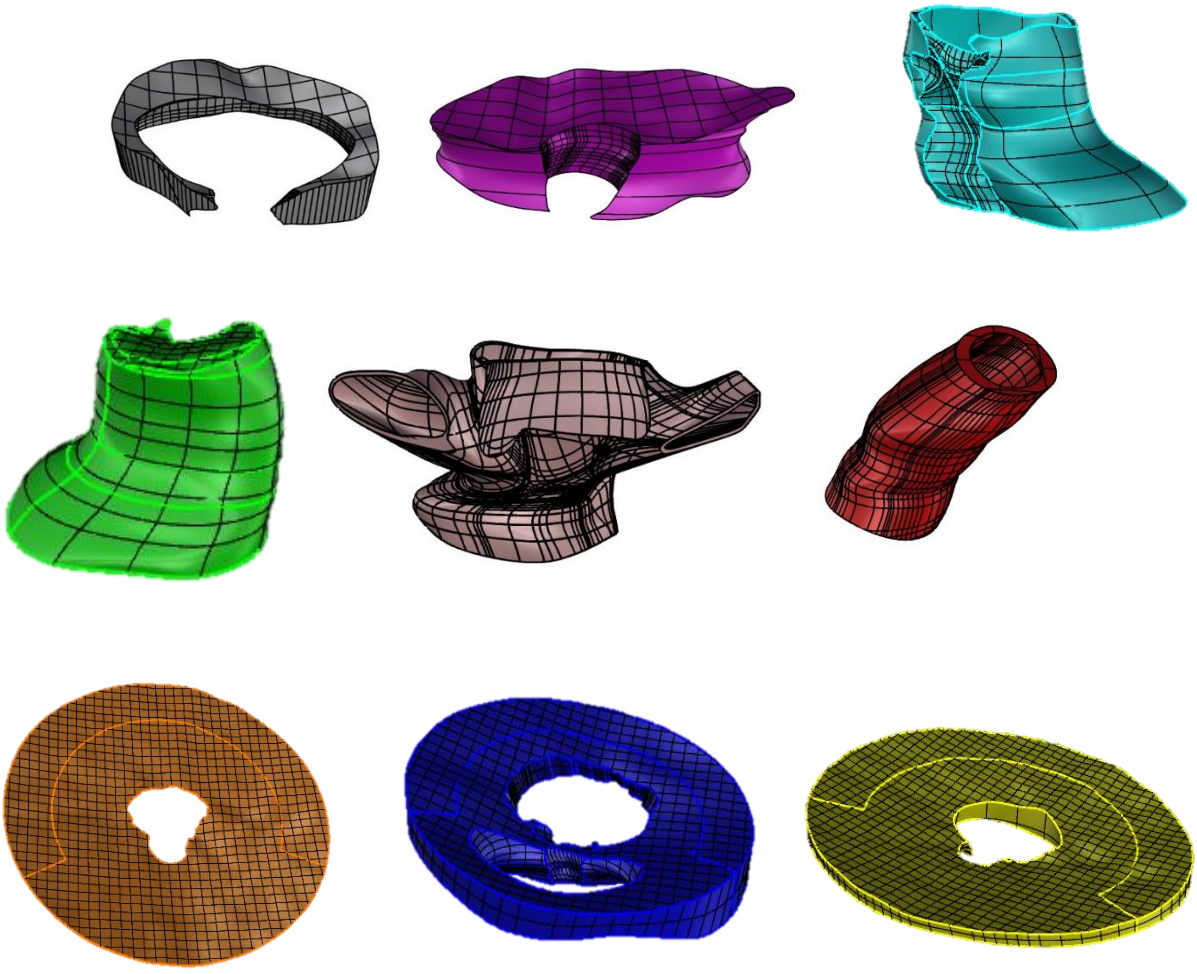

Figure 3.9. All individual water-tight solids after completion. Top row (left to right): PNVP, IAC, and pia. Middle row (left to right): nerve, CRA, and CRV. Bottom row (left to right): BM, sclera, and choroid.

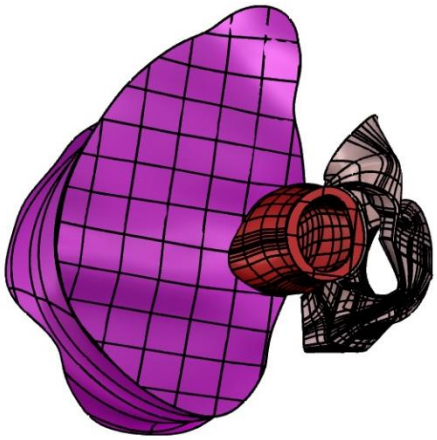

Figure 3.10. Solid IAC (magenta), CRA (red), and CRV (pink). The CRA cuts through the IAC as well as the CRV, making those connecting surfaces flush

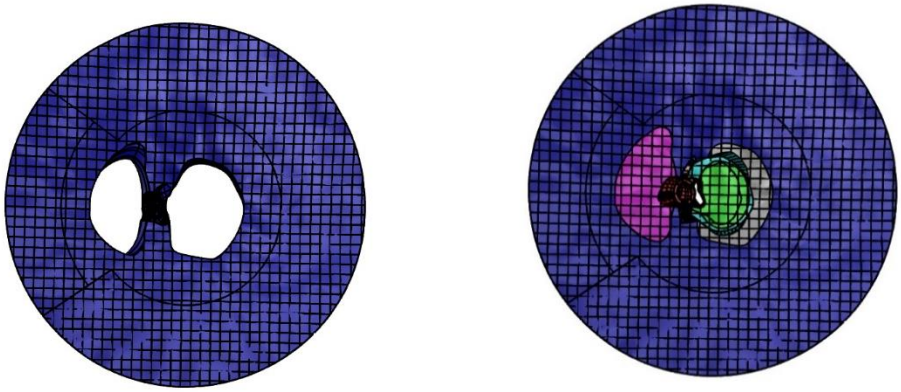

Figure 3.11. Solids cut through the surrounding scleral tissue (blue).

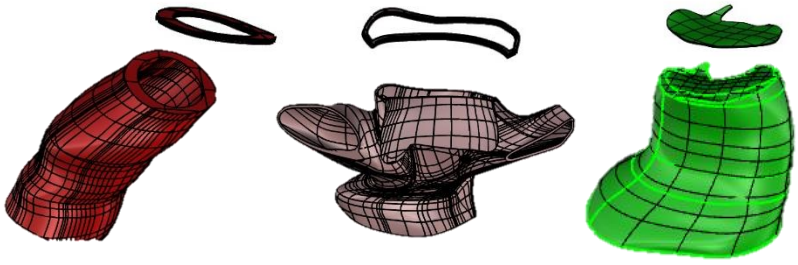

Figure 3.12. Offsetting of anterior solid surfaces to create BM-level solids: (Left to Right) CRA, CRV, nerve.

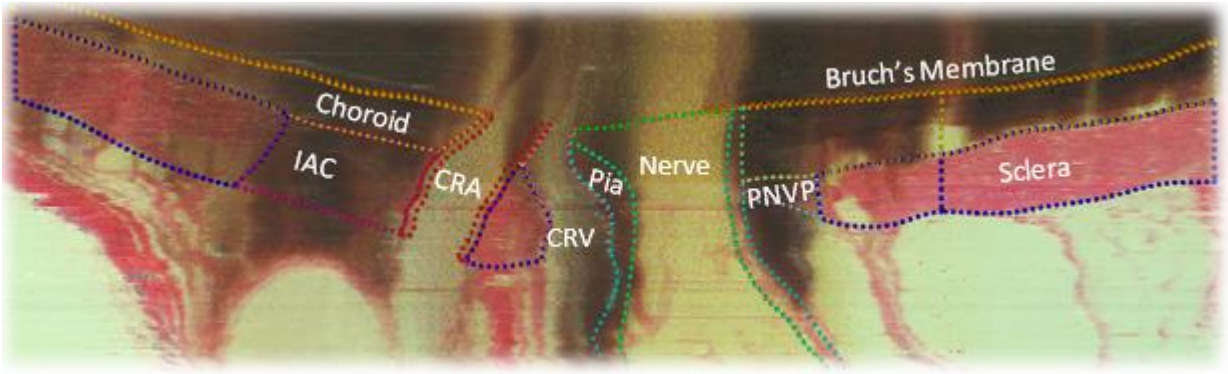

Figure 3.13. Assessment of model geometry by projection of points back onto original histology slide.

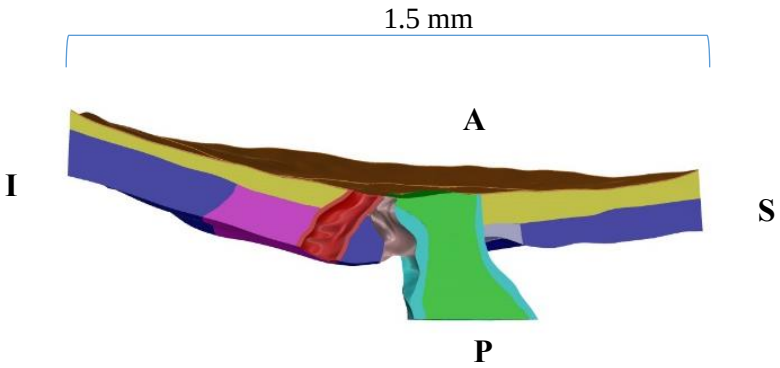

Figure 3.14. Final model including all volumes: PNVP (grey), pia (aqua), CRV (pink), CRA (red), nerve (green), IAC (magenta), choroid (yellow), and BM (orange).

3.1.2.3 Meshing

All individual solids from Rhino were imported into Trelis 16.3.6 for meshing (Computation Simulation Software, LLC). Tissues that were flush, such as the choroid and the sclera, needed to be "merged," allowing Trelis to recognize that they have common surfaces. This ensured that the nodes between the meshes of adjacent tissues aligned, allowing load to be transferred between them during the FE analysis. Each coincident tissue curve and surface was individually merged using various Trelis commands. The outer region of the model, which includes sections of the sclera, BM, and choroid, was meshed with 8-node hexahedral elements, using Map and Sweep meshing schemes (see Figure 3.12). The inner region of BM was meshed with 6-node wedge elements. The thin, anterior regions of the CRV, CRA, and nerve were

meshed with 6-node wedge elements. The remaining tissues were meshed with 4-node tetrahedral elements.

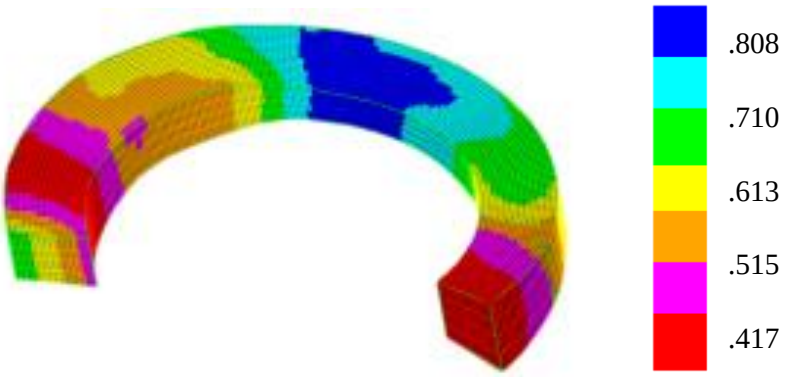

Figure 3.15. Outer sclera meshed with hexahedral elements on Trelis. The color bar represents mesh quality for each element, with 0 representing a poor mesh and a 1 representing a perfect mesh. A higher mesh quality results in better numerical convergence by the FE analysis. We found that a threshold element quality of 0.3 works well for model convergence.

3.1.3 Model Simulation

The meshed model was exported from Trelis to Abaqus 2016 (Dassault Systèmes). A submodeling approach was utilized to apply boundary conditions to the ONH model. Briefly, a posterior eye model with simplified ONH geometry was previously built and solved at an IOP of 20 mmHg. The geometry of the posterior eye model fully enveloped the geometry of the ONH model. In order to set boundary conditions, the posterior half of the eye was analyzed as a global model. The global node displacements were then mapped onto the nodal boundaries of the submodel, the ONH area. The model was simulated with 20 mmHg of IOP on the anterior surfaces of the BM and the BM portions of the CRV, CRA, and nerve. 20 mmHg and 70 mmHg of blood pressure was placed on the interior lumen of the CRV and CRV respectively.

For the initial strain pattern analysis, a baseline model was simulated. For the sensitivity analysis, each tissue stiffness was varied independently, and the model was simulated for both a high and low Young's Modulus.

3.2 Data Analysis

3.2.1 Strain Patterns

Analysis of the data included a qualitative look at how IOP induced strain within the ONH. We also examined the first and third principal strains in the anterior region of the optic nerve (the region from the BM to 150 microns posterior). Under our model assumptions these strains represent the maximum tension and compression experienced in the optic nerve. Specifically, we assessed the average and 95th percentile for first principal strain and average and 5th percentile for the third principal strain. The 95th and 5th percentile strains are chosen because they are less likely than the 1st and 100th percentile strains to be affected by numerical errors such as those resulting from poor element quality. This analysis was performed with the model simulated at baseline YM values for each tissue.

3.2.2 Sensitivity Analysis

The sensitivity analysis on the rat ONH model involved varying the material properties of ONH tissues to determine their influence on the strain in the optic nerve head under increased IOP. For each tissue, the model was simulated twice with a YM above and below the baseline value.

3.2.2.1 Variable Selections

Tissues were modeled as neo-Hookean, isotropic solids. All tissues were assumed to be nearly incompressible and given a Poisson's ratio of 0.49. The Young's modulus (YM) was the varied material property. For each tissue, the model was simulated an additional two times with varied YM values. The YM for each tissue was varied from a baseline stiffness value to a "soft" and "stiff" value and (1/3 baseline and 3 times baseline, respectively). Since material properties specific to the rat ONH are not yet available, material properties were selected based on values

reported in the literature from previous modeling studies on the human ONH [14]. The baseline YM for the tissues were set as follows:

Table 3.1: Baseline Young's Modulus of ONH Tissues

Tissue	**Young's Modulus (MPa)**	**Tissue**	**Young's Modulus (MPa)**
Sclera	3.0	Choroid	0.1
Pia	3.0	PNVP	0.1
BM	7.0	IAC	0.1
CRA and CRV walls	0.3	Nerve	0.03

3.2.2.2 Tissue Influence Ranking

In this sensitivity analysis, we determined the relative sensitivity of strain in the optic nerve to changes in the stiffness values of each tissue. To do so, we selected three YM values for each tissue: "soft", baseline, and "stiff." We first solved a baseline model by setting the YM of all tissues to their baseline values. We then solved a model iteration for every soft and stiff tissue modulus value, resulting in 18 additional variations of the model. The four output measures we calculated were the 95^{th} percentile first principal strain, average first principal strain, 5^{th} percentile third principal strain, and average third principal strain in the anterior optic nerve. For each tissue, we found the absolute response of each output measure by finding its total range (maximum - minimum) across that tissue's YM value iterations. A total response for each tissue was obtained by summing the four absolute response values. Percentage of total influence for each tissue was calculated by dividing the individual tissue's total response by the sum of all tissue total response values. The influence of each tissue stiffness was ranked based on this percentage.

4 RESULTS

4.1 Individual Specific Model

The individual specific model showed high strain concentrations on the inferior side of the nerve, near the central retinal vessels. There were also high strain concentrations on the posterior portion of the PNVP, especially on the superior side. As shown in Table 4.1, the average first and third principle strains in the nerve were 4.6% and -6.1%, with 95th and 5th percentile strains of 7.4% and -9.8% respectively. Figure 4.1 shows three views of the ONH model under a simulated IOP of 20 mmHg with colors representing logarithmic strain values.

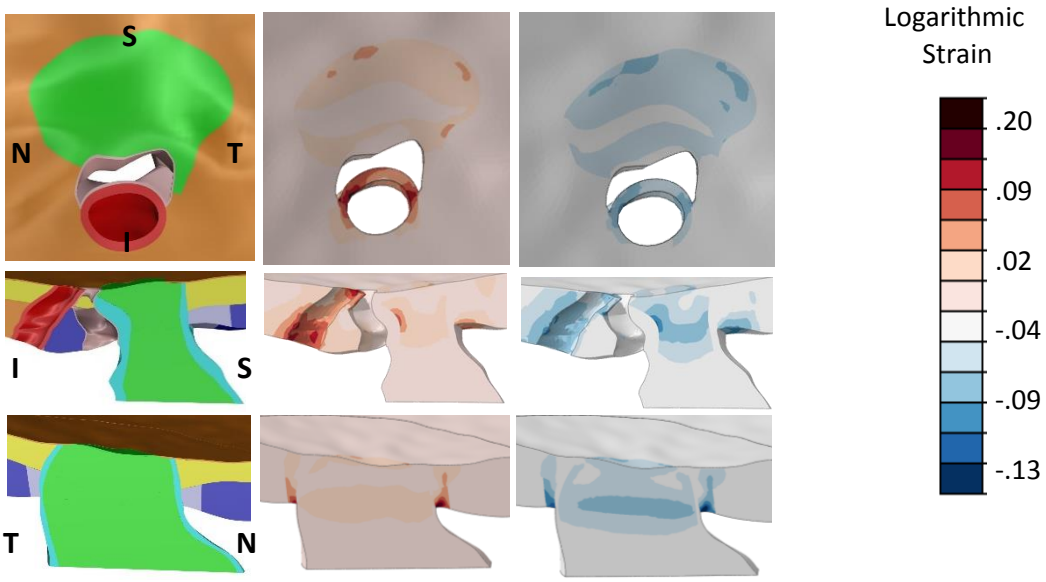

Figure 4.1. Strain patterns in the rat ONH model. Top row shows an en face view. Middle row shows a superior-inferior cut plane view. Bottom row shows a nasal-temporal cut plane view. Left column shows tissues in the model: sclera (blue), choroid (yellow), CRA (red), CRV (pink), PNVP (grey), BM (orange), and nerve (green). Middle column shows first principal, or tensile, strains. Right column shows third principal, or compressive, strains.

Table 4.1: Strain values in the optic nerve tissue. 95th percentile first principal and 5th percentile third principal strains represent maximum tension and compression respectively

	Average and (95th percentile) first principal strain	Average and (5th percentile) third principal strain
Optic Nerve	4.6% (7.4%)	-6.1% (-9.8%)

4.2 Sensitivity Analysis

In general, lowering the YM, or softening, the tissues increased the average and maximum strains in the nerve. We found that scleral stiffness was the most influential on ONH strains, while the vessels and IAC did not have much effect. Additionally, the PNVP had a fair amount of influence, ranking one below the pia. Figure 4.2 is a pie graph illustrating relative tissue influence on strains in the ONH.

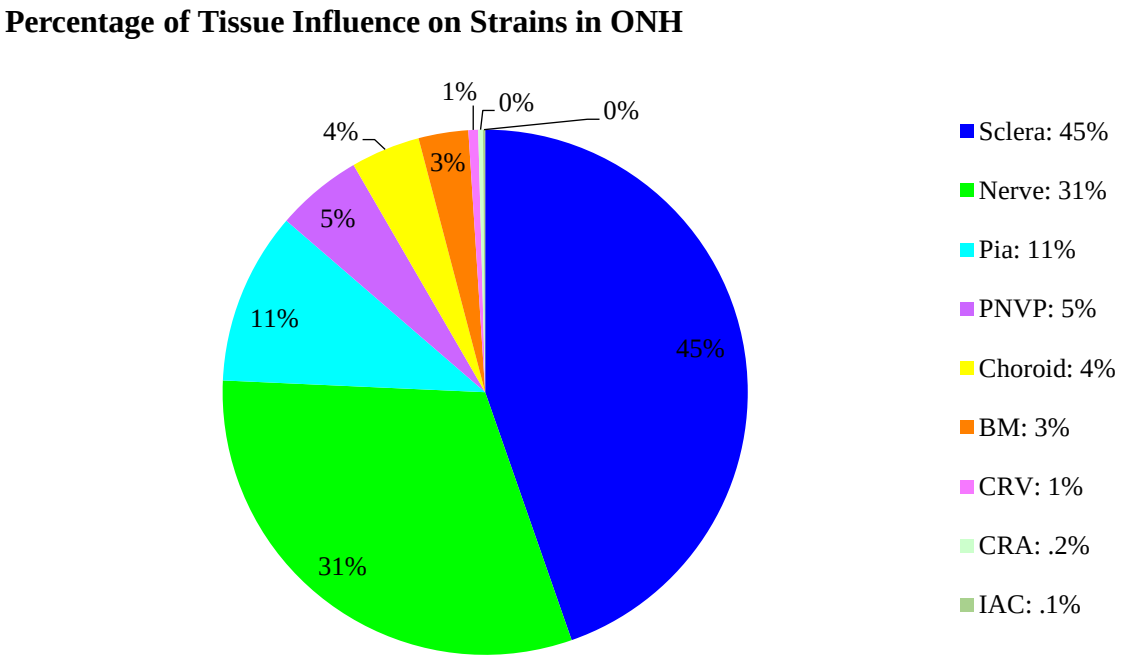

Figure 4.2. This graph illustrates the percentage of influence of each material on the principal strains in the optic nerve head tissue. A higher percentage indicates that tissue's respective stiffness has a higher effect on anterior nerve strains. Tissues on the right are ranked from most to least influential.

5 DISCUSSION

5.1 Individual Specific Model

5.1.1 Strain Patterns

It was expected that the differences in rat and human ONH anatomy would also correlate to differences in high strain areas under elevated pressure, and these areas of high strain are of interest as they indicate possible points of damage during elevated IOP. Unlike human ONH vasculature, the CRV and CRA in the rat ONH are placed inferiorly from the nerve as they leave the globe. This critical difference could explain the high strain concentration on the inferior section of the rat nerve on the side of the main vasculature. It could also be explained by the addition of the IAC, which is located inferior from the CRA and exists only in the rat anatomy.

An additional crucial architectural difference between human and rat anatomy is the lack of a collagenous lamina cribrosa. Without this structural support, it is expected that the strain in this area may be higher than that of a human. The rat ONH model had similar strains to those seen in human modeling studies, even though the human models were simulated with higher IOP levels (50 mmHg compared to 20 mmHg) [12].

The jutting of the BM into the superior side of the nerve was expected to lead to a high strain concentration around the interface of that connection, as the BM was modeled as a much stiffer tissue (7.0 MPa) compared to the nerve (0.03 MPa). However, there does not appear to be a substantially large strain concentration in the superior region of the nerve.

5.1.2 Sensitivity Analysis

The sensitivity analysis indicates that scleral stiffness is the most influential material property on ONH strain. This makes intuitive sense as the sclera is the main load bearing tissue of the eye. This result is also consistent with previous sensitivity studies on the human ONHs. This

adds some support to the suitability of the rat as an animal model for studying the biomechanics of glaucoma in the ONH [14]. However, multiple rat ONHs would need to be assessed to better understand how the anatomical differences between the human and rat ONH may impact the strain distributions. Though the choroid is a larger tissue than the PNVP, it has a lower relative influence on ONH strain. This could be due to the placement of the plexus, as it serves as the circumferential connection between the pia mater and the highest load bearing tissue, the sclera. The rankings of the other vessels are similar to those determined by Sigal et. al in human ONH studies [16].

5.2 Limitations

Due to the sheer complexity of the rat ONH environment and residing tissues, modeling such a structure requires some assumptions and simplifications that may have an overall effect on the results. This individual specific model was chosen to have material properties derived from literature. Though these values are backed by sufficient evidence, these material properties are not individual specific, and modifying these values could lead to changes in strain patterns or total influences of tissues. Furthermore, tissues were modeled as neo-Hookean, isotropic materials and thus essentially linearly elastic; in reality, these tissues are anisotropic and exhibit nonlinear stiffening behavior. Further studies with more realistic material properties could possibly yield different results that would more accurately represent biomechanical analysis of the rat ONH tissues. Additionally, future studies could include a mesh density analysis to ensure that our models have reached numerical convergence.

6 CONCLUSION

As expected, the rat ONH model reported higher strains and more asymmetric strain patterns than those of human ONH models. However, the relative tissue influences for both the rat and human ONH remained similar, with the scleral stiffness being the most influential material property. Thus, the characterization of the rat model provides insight about the biomechanical effect of anatomical differences between rat and human ONHs. In future work the strain patterns in rat ONH models will be compared to biological patterns in experimental rat studies of glaucoma to learn more about the connection between biomechanical insults and RGC death in glaucoma, leading to the identification of targets for novel therapies.

7 REFERENCES

[1] Y. C. Tham, X. Li, T. Y. Wong, H. A. Quigley, T. Aung, and C. Y. Cheng, "Global prevalence of glaucoma and projections of glaucoma burden through 2040: A systematic review and meta-analysis," Ophthalmology, vol. 121, no. 11, pp. 2081–2090, 2014.

[2] J. C. Morrison, M. E. Dorman-Pease, G. R. Dunkelberger, and H. A. Quigley, "Optic Nerve Head Extracellular Matrix in Primary Optic Atrophy and Experimental Glaucoma," Arch Ophthalmol, vol. 108, no. 7, pp. 1020–1024, 1990.

[3] H. a Quigley and E. M. Addicks, "Chronic experimental glaucoma in primates. II. Effect of extended intraocular pressure elevation on optic nerve head and axonal transport," Invest Ophthalmol Vis Sci, vol. 19, pp. 137–152, 1980.

[4] H. Yang, J. C. Downs, C. Girkin, L. Sakata, A. Bellezza, H. Thompson, and C. F. Burgoyne, "3-D Histomorphometry of the Normal and Early Glaucomatous Monkey Optic Nerve Head: Lamina Cribrosa and Peripapillary Scleral Position and Thickness," Investig. Opthalmology Vis. Sci., vol. 48, no. 10, p. 4597, 2007.

[5] C. R. Ethier and C. a. Simmons, Introductory Biomechanics: From Cells to Organisms. 2007

[6] E. C. Johnson, L. M. H. Deppmeier, S. K. F. Wentzien, I. Hsu, and J. C. Morrison, "Chronology of Optic Nerve Head and Retinal Responses to Elevated Intraocular Pressure," IOVS, vol. 41, no. 2, 2000.

[7] M. E. Pease, S. J. McKinnon, H. a. Quigley, L. a. Kerrigan-Baumrind, and D. J. Zack, "Obstructed axonal transport of BDNF and its receptor TrkB in experimental glaucoma," Investig. Ophthalmol. Vis. Sci., vol. 41, no. 3, pp. 764–774, 2000.

[8] J. C. Morrison, W. O. Cepurna Ying Guo, and E. C. Johnson, "Pathophysiology of human glaucomatous optic nerve damage: Insights from rodent models of glaucoma," Exp. Eye Res., vol. 93, no. 2, pp. 156–164, 2011.

[9] H. A. Quigley and E. M. Addicks, "Regional differences in the structure of the lamina cribrosa and their relation to glaucomatous optic nerve damage," Arch Ophthalmol, vol. 99, no. 1, pp. 137–143, 1981.

[10] Morrison, J. C., Cepurna Ying Guo, W. O., & Johnson, E. C. (2011). Pathophysiology of human glaucomatous optic nerve damage: insights from rodent models of glaucoma. *Exp Eye Res, 93*(2), 156-164.

[11] Sigal, I. A., Flanagan, J. G., Tertinegg, I., & Ethier, C. R. (2004). Finite element modeling

of optic nerve head biomechanics. *Invest Ophthalmol Vis Sci, 45*(12), 4378-4387. doi:10.1167/iovs.04-0133

[12] Sigal, I. A., Flanagan, J. G., Tertinegg, I., & Ethier, C. R. (2009). Modeling individual-specific human optic nerve head biomechanics. Part I: IOP-induced deformations and influence of geometry. *Biomechanics and Modeling*

[13] Kang, M. H., & Yu, D. Y. (2015). Distribution pattern of axonal cytoskeleton proteins in the human optic nerve head. *Neural Regen Res, 10*(8), 1198-1200. doi:10.4103/1673-5374.162691

[14] Sigal, I. A., Flanagan, J. G., & Ethier, C. R. (2005). Factors influencing optic nerve head biomechanics. *Invest Ophthalmol Vis Sci, 46*(11), 4189-4199. doi:10.1167/iovs.05-0541

[15] Pazos M, Yang H, Gardiner SK, et al. Rat Optic Nerve Head Anatomy within 3D Histomorphometric Reconstructions of Normal Control Eyes. *Experimental Eye Research*. 2015;139:1-12. doi:10.1016/j.exer.2015.05.011.

[16] Sigal, I. A., Flanagan, J. G., Tertinegg, I., & Ethier, C. R. "Modeling individual-specific human optic nerve head biomechanics. Part II: Influence of material properties," Biomech. Model. Mechanobiol., vol. 8, no. 2, pp. 99–109, 2009.

[17] Downs JC, Yang H, Girkin C, et al. Three-dimensional histomorphometry of the normal and early glaucomatous monkey optic nerve head: Neural canal and subarachnoid space architecture. *Investig Ophthalmol Vis Sci*. 2007;48(7):3195-3208. doi:10.1167/iovs.07-0021.